Lymph Nodes

2

Sugoto Mukherjee, Mark J. Jameson, Max Wintermark, and Prashant Raghavan

2.1 Introduction

While there are a variety of causes of cervical lymphadenopathy (see Box 2.1), the primary role for imaging in cervical lymphadenopathy is to diagnose metastatic disease in head and neck squamous cell carcinoma (HNSCC), which significantly impacts treatment. Other nonneoplastic causes of cervical lymphadenopathy, including various infectious and inflammatory diseases, usually do not require routine imaging. This chapter reviews the anatomy and classification of cervical lymph nodes, diagnostic criteria, and imaging findings of lymph node metastasis and the imaging appearance of other benign cervical lymphadenopathies.

Box 2.1. Causes of Cervical Lymphadenopathy

Neoplastic	Squamous cell carcinoma
	Lymphoma
	Thyroid carcinoma (papillary most common)
	Kaposi sarcoma
	Metastases (lung, breast, melanoma, renal cell, carcinoid)
Infection	Bacterial
	Mycobacterium tuberculosis
	Infectious mononucleosis
	Cytomegalovirus
	Rubella
	Cat-scratch disease
	Brucellosis
	Lyme disease
Granulomatous disease	Sarcoidosis
	Langerhans cell histiocytosis
Miscellaneous	Castleman's disease (angiofollicular lymphoid hyperplasia)
	Posttransplantation lymphoproliferative disease
	Sinus histiocytosis with massive lymphadenopathy
	Kimura disease

P. Raghavan et al., *Manual of Head and Neck Imaging*,
DOI 10.1007/978-3-642-40377-4_2, © Springer-Verlag Berlin Heidelberg 2014

2.2 Anatomy and Pathophysiology

Given that regional nodal metastasis is the single most important prognostic factor for HNSCC, evaluation of cervical nodes is an essential component of staging and treatment planning. Cross-sectional imaging significantly improves accuracy of detection of metastatic nodal disease, particularly when non-palpable.

Knowledge of cervical anatomy and nodal classification is essential to accurately describe cervical nodal metastases in HNSCC. The American Joint Committee on Cancer (AJCC) has classified neck lymph nodes from levels I through VII. Level I refers to nodes in the submandibular and submental regions. Levels II, III, and IV refer to lymph nodes along the anterior cervical chain. Level V and VI nodes are in the posterior and visceral compartments of the neck, respectively, and level VII nodes are in the superior mediastinum (Fig. 2.1).

The essential anatomic landmarks used for imaging classification are depicted in Fig. 2.1 and are described in Box 2.2. Certain nodes are still classified according to their anatomic names, including supraclavicular, retropharyngeal, parotid, facial, occipital, and postauricular.

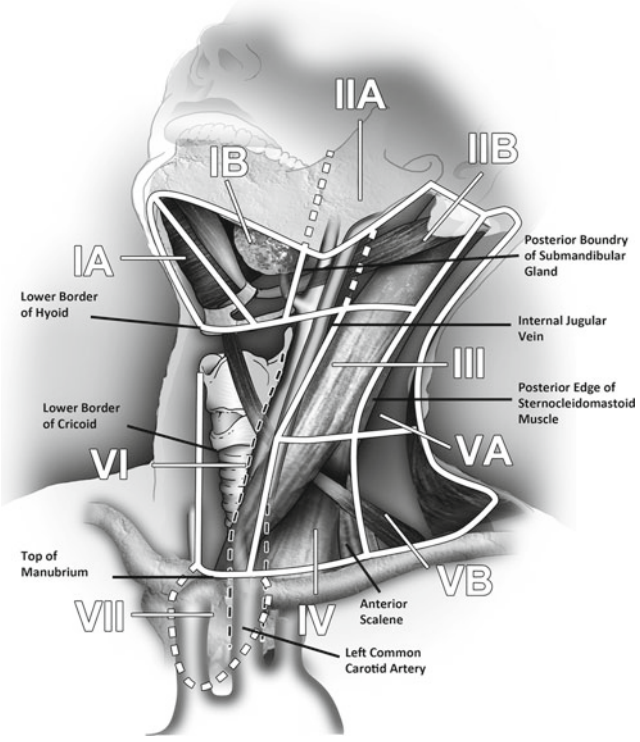

Fig. 2.1 Oblique sagittal graphic showing the relevant anatomic landmarks for imaging-based nodal classification. The important landmarks visible on this graphic include lower border of hyoid (levels *I* and *II*), lower border of cricoid (levels *III* and *IV*), (levels *VA* and *VB*) top of manubrium (levels *VI* and *VII*), anterior belly of digastric (levels *IA* and *IB*), posterior border of submandibular gland (levels *IB* and *IIA*), and posterior border of internal jugular vein (levels *IIA* and *IIB*). The anterior scalene (levels *IV* and *VB*) and carotid arteries (levels *II* and *IV* from *VI*) are not well visualized on this image

Box 2.2. Imaging-Based Nodal Classification

Levels	Boundaries			
	Superior	Inferior	Anterior (medial)	Posterior (lateral)
IA Submental group	Symphysis of mandible	Body of hyoid	Anterior belly of contralateral digastric muscle	Anterior belly of ipsilateral digastric muscle
IB Submandibular group	Body of mandible	Posterior belly of digastric muscle	Anterior belly of digastric muscle	Stylohyoid muscle
IIA Upper jugular group nodes	Skull base	Horizontal plane defined by the inferior border of hyoid bone	Stylohyoid muscle	Vertical plane defined by the spinal accessory nerve
IIB Upper jugular group nodes	Skull base	Horizontal plane defined by the inferior border of hyoid bone	Vertical plane defined by the spinal accessory nerve	Lateral border of the sternocleidomastoid muscle
III Mid-jugular group	Horizontal plane defined by the inferior border of hyoid bone	Horizontal plane defined by the inferior border of cricoid cartilage	Lateral border of the sternohyoid muscle	Lateral border of the sternocleidomastoid muscle or sensory branches of the cervical plexus
IV Lower jugular group	Horizontal plane defined by the inferior border of cricoid cartilage	Clavicle	Lateral border of the sternohyoid muscle	Lateral border of the sternocleidomastoid muscle or sensory branches of the cervical plexus
VA Posterior triangle group	Apex of the convergence of sternocleido-mastoid and trapezius muscles	Horizontal plane defined by the inferior border of the cricoid cartilage	Lateral border of the sternocleido-mastoid muscle or sensory branches of the cervical plexus	Anterior border of the trapezius muscle
VB Posterior triangle group	Horizontal plane defined by the inferior border of cricoid cartilage	Clavicle	Lateral border of the sternocleido-mastoid muscle or sensory branches of the cervical plexus	Anterior border of the trapezius muscle

Levels	Boundaries			
	Superior	Inferior	Anterior (medial)	Posterior (lateral)
VI Central or anterior group	Hyoid bone	Top of manubrium	Common carotid artery	Common carotid artery
VII Superior mediastinal group	Top of manubrium	Innominate vein	Common carotid artery	Common carotid artery

Note: Other superficial nodal groups continue to be referred to by their anatomic names including parotid, facial, and postauricular lymph nodes

The clinically important internal jugular nodes are classified as level II, III, or IV nodes (previously referred to as upper, mid-, and lower jugular nodes). On axial imaging, levels II and III are separated by the bottom of the body of the hyoid bone, and levels III and IV are separated by the bottom of the arch (anterior rim) of the cricoid cartilage (Figs. 2.2 and 2.3). All three levels are bounded posteriorly by the posterior edge of sternocleidomastoid muscle (SCM). Level II is also bounded posteriorly by the posterior edge of the submandibular gland. Level IIA nodes lie adjacent to the internal jugular vein (IJV); any level II nodes that are posterior to the IJV and are separated from the vein by a fat plane are level IIB nodes. Level I nodes are above the hyoid bone, below the mylohyoid muscle, and anterior to posterior margin of submandibular gland. They are subdivided into levels IA (submental) and IB (submandibular) based on whether they are medial or posterolateral to the anterior belly of digastric muscle, respectively. Level III nodes lie anterior to the posterior margin of the SCM and in between the lower margin of the body of the hyoid bone and the lower margin of the cricoid cartilage arch. Level III nodes also lie lateral to the medial margin of either the common carotid artery or the internal carotid artery. On each side of the neck, the medial margin of these arteries separates level III (lateral) from level VI (medial) nodes. Level IV nodes lie between the level of the lower margin of the cricoid cartilage arch and the level of the clavicle as seen on each axial scan. These nodes are anteromedial to a line drawn through the posterior edge of the SCM and the posterolateral edge of the anterior scalene muscle on each axial image. Also, the medial aspect of the common carotid artery separates level IV (lateral to the artery) from level VI nodes (medial to the artery) (Figs. 2.1 and 2.4).

Level V nodes extend from the skull base, at the posterior border of the attachment of the SCM, to the level of the clavicle as seen on each axial scan. Level VA (upper level V) nodes lie between the skull base and the lower margin of the cricoid cartilage arch, behind the posterior edge of the SCM, while level VB (lower level V) nodes lie between the level of the lower margin of the cricoid cartilage arch and the level of the clavicle as seen on each axial scan. Their anterior boundary if formed by the posterior edge of the SCM (Figs. 2.1, 2.2, and 2.3).

Identification of the clavicle allows one to separate the supraclavicular from axillary nodes on axial CT slices. When any portion of the clavicle is seen on the scan, the visible nodes are classified as supraclavicular nodes, while any nodes below the level of the clavicle and lateral to the ribs are classified as axillary nodes.

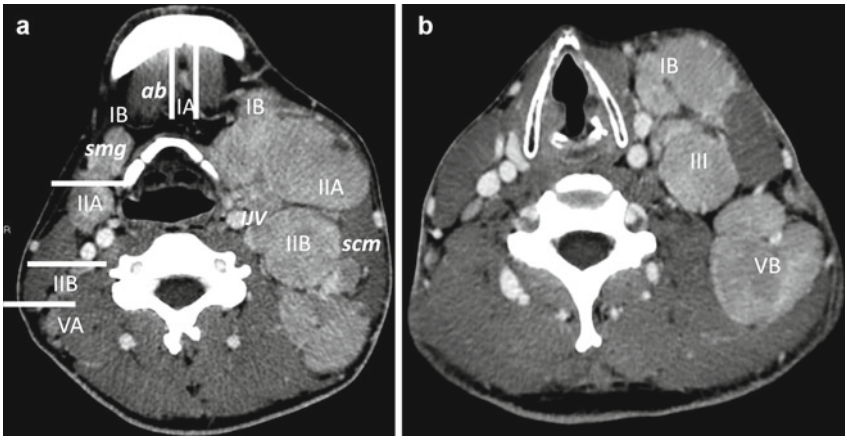

Fig. 2.2 (**a** and **b**) A 23 year-old with Hodgkin's lymphoma above and below the hyoid cartilage. *ab* anterior belly of digastric, *smg* submandibular gland, *scm* sternocleidomastoid, *IJV* internal jugular vein. *White lines* divide the different nodal compartments. Level *IA* is in between the anterior belly of digastric, while level *IB* is in between the anterior belly of digastric and posterior margin of submandibular gland. Levels *II/III/IV* are separated from level *V* by posterior border of sternocleidomastoid. Levels *IIA* and *IIB* are divided by internal jugular vein (*IJV*). Nodes that lie anterior or contact IJV are *IIA* nodes. Levels *II* and *III* and *III* and *IV* are defined by the inferior borders of hyoid and cricoid cartilages, respectively

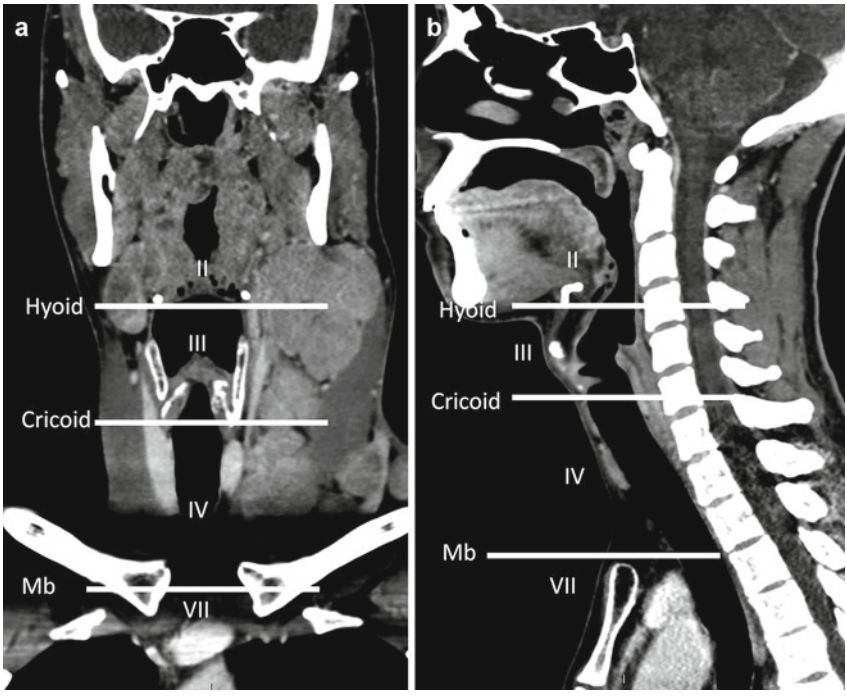

Fig. 2.3 (**a** and **b**) Coronal and sagittal CT images show levels *II*, *III*, and *IV* sites divided by inferior border of hyoid and inferior border of cricoid. Levels *VI* and *VII* are separated by the superior border of manubrium

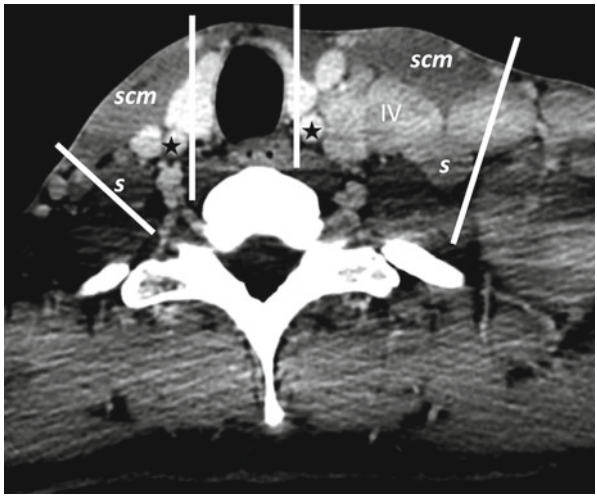

Fig. 2.4 Axial contrast-enhanced CT scans through the infrahyoid lower neck show levels IV, V, and VI sites, defined by medial margin of common carotid artery (*star*) and oblique line from lateral anterior scalene muscle (*s*) to posterior border of sternocleidomastoid muscle (*scm*)

Level VI nodes or the visceral nodes lie inferior to the lower body of the hyoid bone, superior to the top of the manubrium, and between the medial margins of the left and right common carotid arteries or the internal carotid arteries. Level VII nodes lie inferior to the top of the manubrium in the superior mediastinum, between the medial margins of the common carotid arteries. These superior mediastinal nodes extend caudally to the level of the innominate vein (Figs. 2.3 and 2.4).

2.3 Imaging Evaluation

2.3.1 CT and MRI

On imaging, the radiologist needs to identify the pathological nodes based on size, shape, and abnormal nodal architecture. Laterality (ipsilateral, contralateral, or bilateral) must also be noted. Other important features that affect management such as the presence of extracapsular spread of tumor, carotid encasement, and fixation of the tumor to the skull base or prevertebral space also needs to be identified and mentioned. According to the 50 % rule for pathological nodes, presence of nodal metastases decreases the patient's morbidity and mortality by 50 %; presence of bilateral nodes, extracapsular spread, and nodal fixation each lowers the prognosis by an additional 50 %.

The established size criteria for pathological lymph nodes are somewhat arbitrary and controversial and vary among different institutions and practitioners. A commonly used set of size criteria places cutoffs of ≥1.5 cm for levels I and II, ≥1 cm for levels III–V, and ≥8 mm for retropharyngeal nodes (Fig. 2.5). However, many malignant nodes are normal in size, whereas enlarged nodes may be benign. Malignant lymph nodes appear more rounded as compared to benign nodes, which are bean-shaped. Thus, another criterion is based on the ratio of long-axis to

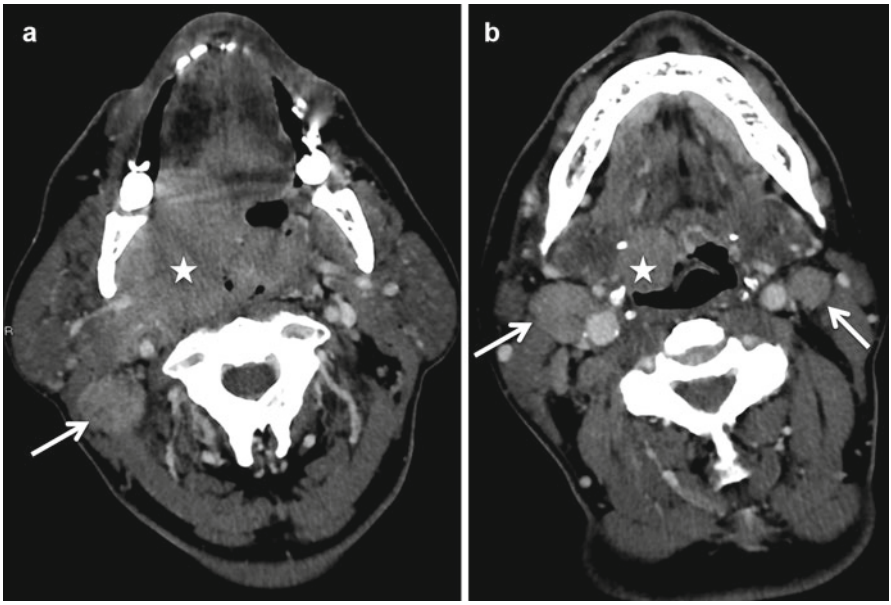

Fig. 2.5 Large T4b invasive tonsillar tumor (*star*) with bilateral pathological adenopathy. Note the rounded shape with loss of internal hilar fat of these enlarged right level IIB (*arrow* in **a**) and bilateral IIA nodes (*arrows* in **b**)

short-axis measurements, with a ratio >2 favoring a benign node and a ratio <2 being concerning for malignancy. Size criteria alone are not reliable, with a false-positive and false-negative rates of ranging from 15 to 20 %. Retropharyngeal lymph nodes are always abnormal when necrotic in the setting of cancer, irrespective of their size (Fig. 2.6). Intraparotid lymph nodes should be suspected to be abnormal in the setting of scalp skin malignancies (Fig. 2.7).

For neck nodes, the presence of hilar fat (easily identified on CT or MR) indicates benignity; this should be distinguished from necrosis, which is usually centrally located in a rounded node (Fig. 2.8). In patients with HNSCC, nodal necrosis implies regional metastasis until proven otherwise. Necrotic nodes can appear cystic when the intranodal contents demonstrate fluid-like imaging appearance with a thin enhancing wall; this is particularly common with human papillomavirus (HPV)-related HNSCC, and the inner cystic component can have complex signal characteristics (Fig. 2.9). The likelihood of necrosis in a metastatic lymph node increases with lymph node size, with more than 50 % of nodes ≥1.5 cm demonstrating necrosis. In addition to HNSCC, necrotic or cystic nodes are not uncommonly seen in metastatic papillary thyroid cancer (PTC).

Cervical lymph node calcification (Fig. 2.10) is rare (~1 %). Presence of nodal calcification is not a reliable predictor of either benign or malignant disease; however, it does provide a limited differential diagnosis. Calcification in cervical lymph nodes is most common in PTC and is occasionally seen in metastatic mucinous adenocarcinoma, treated lymphoma, and granulomatous diseases.

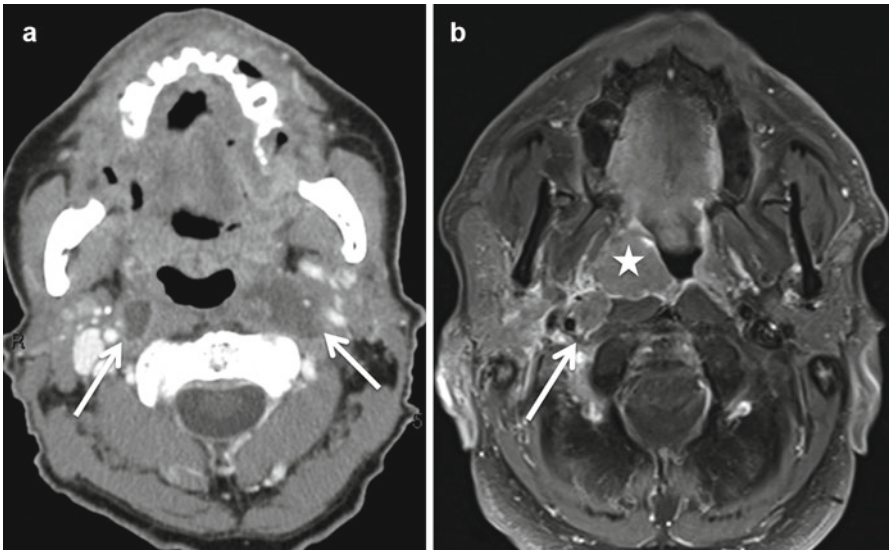

Fig. 2.6 Contrast-enhanced CT (**a**) in a patient with sinonasal tumor demonstrates bilateral necrotic retropharyngeal nodes (*arrows*). Another 55-year-old patient (**b**) with tonsillar cancer (*star*) has a pathological 1 cm right retropharyngeal node (*arrow*)

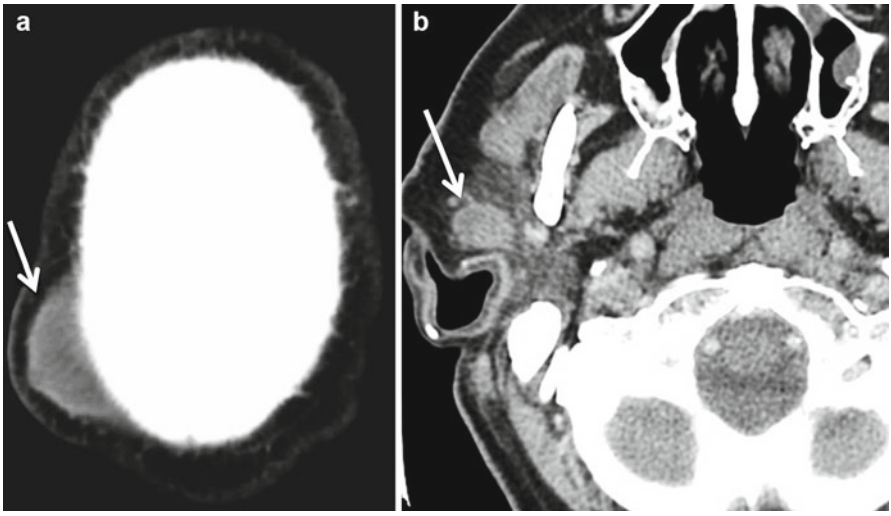

Fig. 2.7 A 65 years old with right vertex squamous cell carcinoma (*arrow* in **a**) with pathological intraparotid adenopathy (*arrow* in **b**). These nodes represent the first echelon of drainage for cutaneous malignancies of the scalp

The presence of extracapsular spread (ECS) of metastatic nodal disease is associated with increased local recurrence rates and decreased survival in patients with HNSCC. Extracapsular extension is identified by poorly defined nodal margins and/

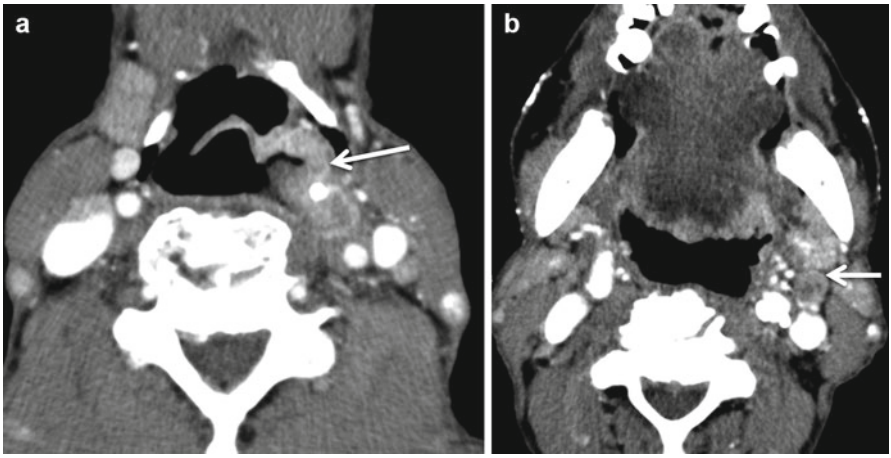

Fig. 2.8 A 55-year-old with left pyriform sinus cancer (*arrow* in **a**) and a pathological left level IIA node (*arrow* in **b**) with loss of hilar fat and central necrosis. Although the level IIA nodes are not pathological by size criteria, the presence of central necrosis along with the known primary suggests that this node is pathological

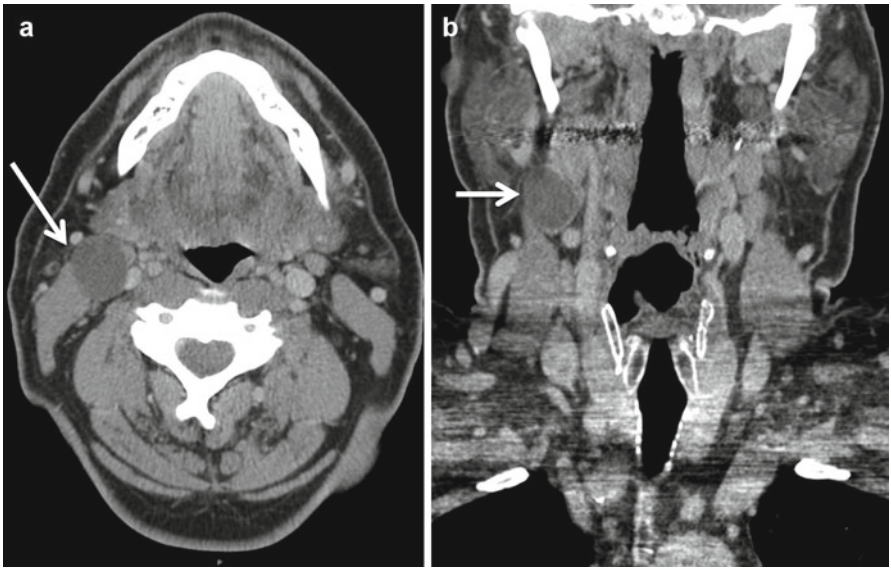

Fig. 2.9 Axial (**a**) and coronal (**b**) contrast-enhanced CT scans in this 52-year-old male with right level II cystic mass (*white arrows*). No primary was identified on endoscopic-guided biopsies. CT-guided FNA showed a metastatic node from a squamous cell carcinoma. This is a common presentation of HPV (human papillomavirus)-associated oral and oropharyngeal cancers which are known for cystic nodal level II metastasis

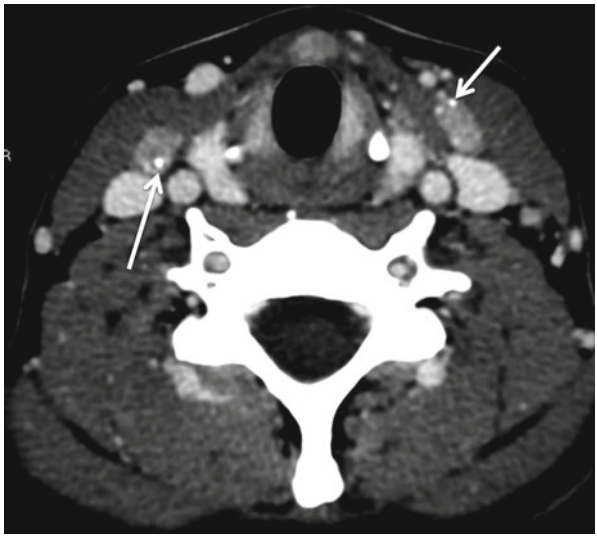

Fig. 2.10 Bilateral pathological level IV enhancing nodes in this patient with papillary carcinoma of the thyroid with small specks of calcification (*arrows*)

or soft tissue infiltration or stranding of the muscles or fat in the neck with loss of normal tissue planes (Fig. 2.11). Also, increasing lymph node size is an indicator of ECS with larger nodes more frequently demonstrating ECS.

Some of the other advanced imaging techniques, which are infrequently used, include diffusion-weighted MRI (DWI), perfusion imaging with dynamic contrast-enhanced MRI (DCE-MRI), and CT perfusion. These techniques, particularly CT and MR perfusion imaging, may allow us to predict biological behavior of these cancers and identify early responders and nonresponders and allow alternative treatment as well as earlier treatment modification.

2.3.2 Ultrasonography

Sonography is used both for detecting nodes and for guiding fine needle aspiration (FNA). A high-frequency linear transducer with Doppler capability is the preferred tool. Normal nodes appear oval/oblong with an echogenic hilum, hypoechoic cortex, and minimal or no intranodal blood flow on color Doppler. Increased short-axis diameter (rounding) and absence of central hilar echogenicity are the criteria most predictive of lymph node metastasis (Fig. 2.12). Doppler imaging can detect peripheral vascularity with or without central vascularity, which significantly improves the overall accuracy of sonography in identifying metastatic nodes. Lymphoma is an exception, as involved nodes may only have hilar flow. Other signs of malignancy include focal or eccentric hypertrophy of the peripheral cortex, absence of an echogenic hilus, indistinct margin (suggests ECS), and necrotic/cystic changes within the substance of the node. Most metastatic nodes appear hypoechoic to adjacent muscle, except for metastatic PTC. US-guided FNA is an extremely reliable and efficient technique to obtain cells for cytologic evaluation and confirmation of suspected metastatic disease and to obtain samples for microbiologic evaluation (Fig. 2.12).

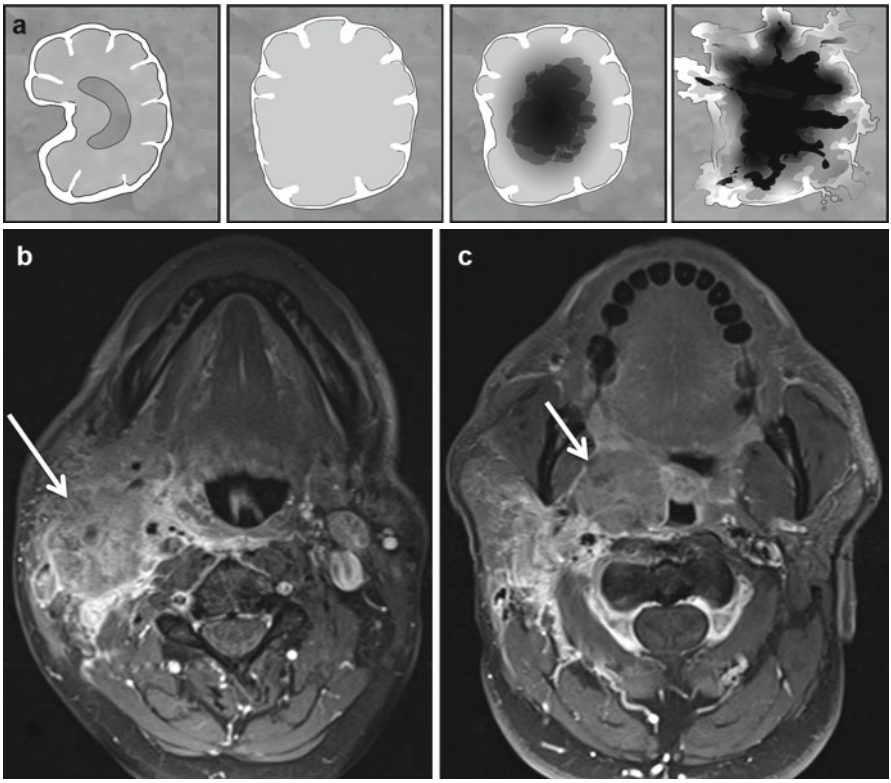

Fig. 2.11 (**a**) Graphic shows the progressive changes in a node when it is involved in metastatic disease. The first image shows the reniform shape of the node, with hilar fat and distinct margins. The involved node loses its normal shape, becomes more rounded followed by central necrosis in the third image. Later stages result in disease spilling out of the node with extracapsular extension. This is seen on imaging as irregular shape, with loss of clear nodal margins and abnormal appearance of the adjacent fat on CT and MR. (**b** and **c**) Axial post-contrast fat-saturated images show extracapsular spread of the right level II nodal mass (*arrow* in **b**) with loss of surrounding tissue planes. The nodal mass has completely infiltrated the right posterior masticator space, the parapharyngeal fat, and possibly the right carotid space. Note the right tonsillar primary (*arrow* in **c**)

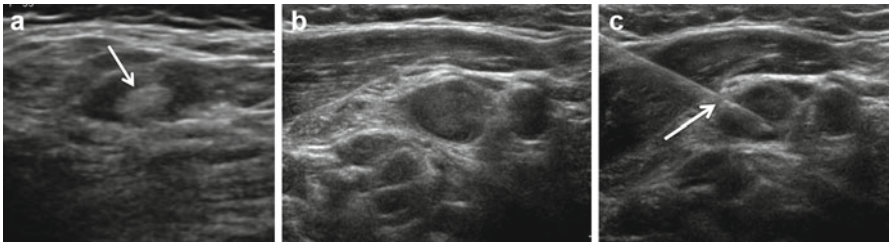

Fig. 2.12 Gray-scale transverse view US image showing a normal lymph node (**a**), with oval shape and echogenic central hilum (*arrow*). Pathological lymph node (**b**) shows a rounded shape with loss of central echogenic fatty hilum, in a patient with thyroid cancer. US (**c**) also helps in providing guidance (*arrow*) for fine needle aspiration cytology and biopsy

2.3.3 PET

Out of various available advanced imaging techniques, 18FDG-PET is most commonly used in clinical practice. FDG-PET has been used in the pretreatment setting for indeterminate nodes on CT/MR, distant metastasis (Fig. 2.13); higher tumor burden with less nodal disease than expected and for baseline scans. FDG-PET is also used for evaluation of residual nodal disease in postradiation setting. Other adjunct uses include directing biopsy/FNA and in patients with unknown primary. Limitations of FDG-PET include false-positive results due to physiological uptake and false negative in necrotic lymph nodes, which may simply not contain sufficient metabolically active tissue to take up FDG.

2.3.4 Posttreatment Evaluation of Residual/Recurrent Nodal Disease

After radiation therapy, routine CT and MR imaging with contrast is insensitive in identifying residual/recurrent nodal disease secondary to scar, fibrosis, and granulation tissue. On a conventional neck CT scan, residual and or recurrent nodal disease may manifest as increasing size or new nodal lesions, as well as persistent intranodal hypodensity (concerning for nodal necrosis). FDG-PET scanning has a role in this setting and can help in identifying residual/recurrent disease in some of these patients (Fig. 2.14).

2.4 Other Pathology

Various other malignancies, infections, and granulomatous/inflammatory diseases can involve neck nodes (Box 2.1), the most common of which are discussed below.

2.4.1 Lymphoma

Lymphoma is the second most common malignancy in the head and neck after squamous cell carcinoma. Hodgkin's disease accounts for 25 % of all lymphomas and extranodal involvement is rare. Non-Hodgkin's lymphoma, however, may present as both nodal and extranodal disease. Lymphoma typically involves deep lymphatic chains, such as the internal jugular, spinal accessory, and transverse cervical chains. Typical imaging reveals one or more well-demarcated homogeneous nodes (Fig. 2.15). Extranodal tumor extension, nodal necrosis, calcification, and hemorrhage are rare but may be seen posttreatment. On MR imaging when compared to muscle, involved nodes are iso- to hypointense on T1-weighted images and hyperintense on T2-weighted images; they exhibit homogenous enhancement. An important caveat here is the protean manifestations of extranodal lymphoma,

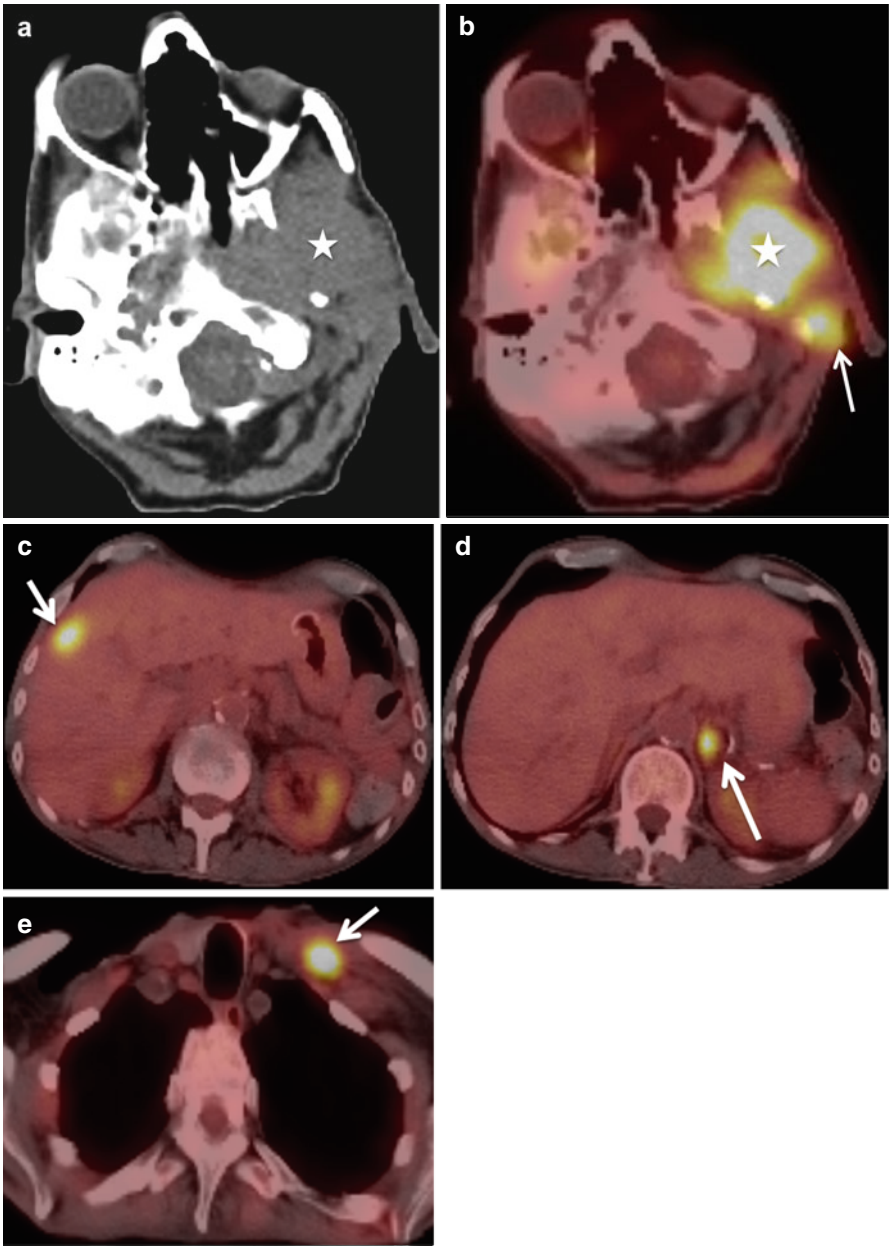

Fig. 2.13 (**a** and **b**) 18FDG-PET scan demonstrates T4b oropharyngeal carcinoma with involvement of the left nasopharynx, left masticator, nasopharyngeal spaces, and the deep lobe of the parotid (*star* in **a** and **b**). A level VA metastatic lymph node is also evident (*arrow* in **b**). (**c**–**e**) Whole body PET scan demonstrated distant metastasis in the left supraclavicular node, right lobe of liver and left adrenal gland (*arrows* in **c**, **d** and **e**)

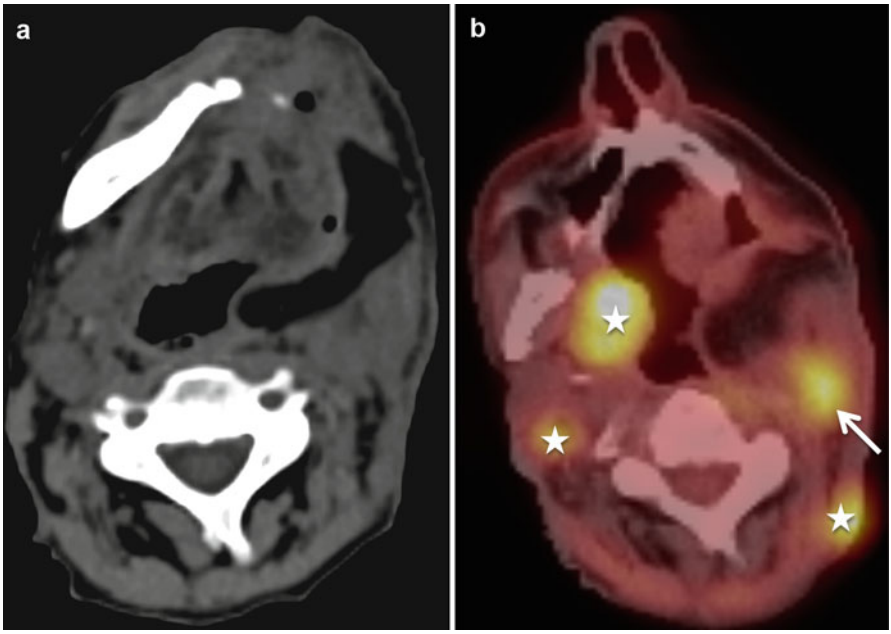

Fig. 2.14 (**a** and **b**) Posttreatment 18FDG-PET scan in this patient status post left hemimandibulectomy, left-sided selective neck dissection, and pectoralis flap reconstruction demonstrates multiple sites of recurrent tumor, both within the postsurgical site (*arrow* in **b**) as well as ipsilateral and contralateral metastatic nodal disease (*star* in **b**)

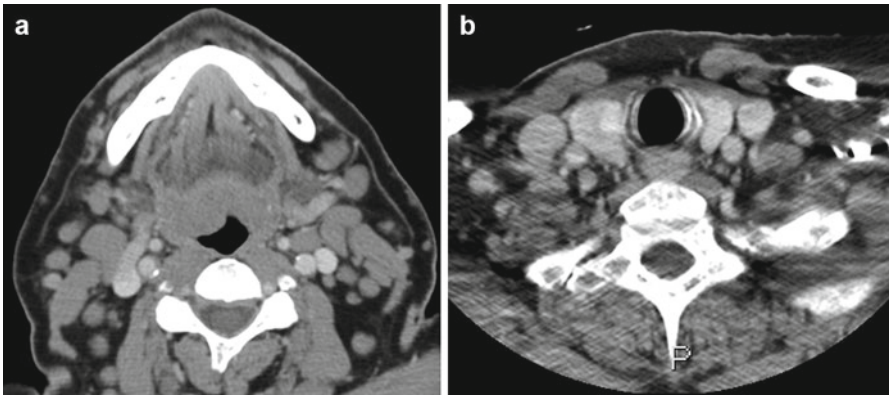

Fig. 2.15 (**a** and **b**) A 55-year-old male with Hodgkin's lymphoma shows multilevel bilateral discrete nodes, both within the suprahyoid and infrahyoid neck. The nodes are rounded with loss of inner hilar fat

which can include infiltrative lesions involving the orbits, nasal cavity, bones, thyroid gland, and/or salivary glands (Fig. 2.16). Extranodal B cell lymphomas can spread along vessels and nerves and can mimic other lesions.

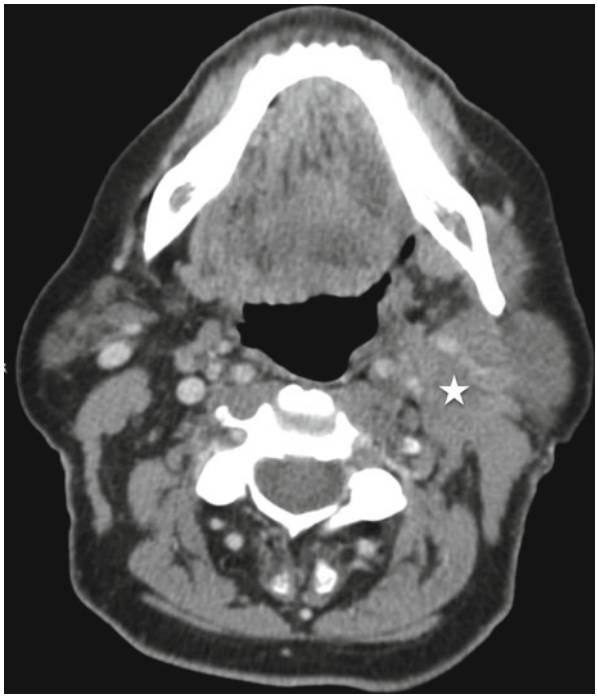

Fig. 2.16 A 55-year-old with diffuse large B cell lymphoma demonstrates an infiltrative mass (*star*) involving the left parapharyngeal space, the left carotid space, and the deep lobe of the left parotid

2.4.2 Papillary Thyroid Carcinoma

Papillary thyroid carcinoma (PTC) frequently metastasizes to cervical lymph nodes. A unique imaging feature of PTC metastases is areas of T1 hyperintensity, which is thought to represent a high concentration of thyroglobulin or intranodal hemorrhage (Fig. 2.17). Other considerations for hemorrhagic nodal disease include metastasis from renal cell carcinoma or melanomas. Nodal calcifications, seen on both CT and ultrasound imaging using high-frequency transducers, can also be seen in metastatic PTC (Fig. 2.18). PTC can also present with purely cystic nodal metastasis.

2.4.3 Bacterial Infection

Many of the infectious causes of cervical lymphadenopathy have a nonspecific imaging appearance. An important imaging feature, which suggests infection rather than neoplasm, is the presence of adjacent fascial thickening and fat infiltration. Suppurative infectious adenopathy can be indistinguishable from malignant necrotic nodal disease, and the clinical context is paramount.

A common clinical scenario is acute nodal enlargement in children, which is frequently due to *S. aureus* infection. An infected node may undergo suppurative necrosis, which manifests as a low-density center surrounded by shaggy enhancement and stranding of the adjacent fat on CT.

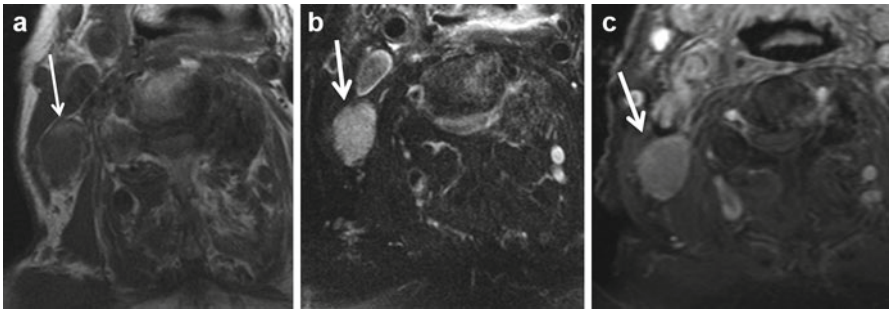

Fig. 2.17 Metastatic right level III lymph node from a papillary thyroid primary. This node is slightly hyperintense, most prominent along the anterior aspect, on the T1-weighted images (*arrow* in **a**) and is hyperintense on the fat-saturated T2-weighted image (*arrow* in **b**). It demonstrates homogeneous enhancement on the post-contrast fat-suppressed T1-weighted image (*arrow* in **c**)

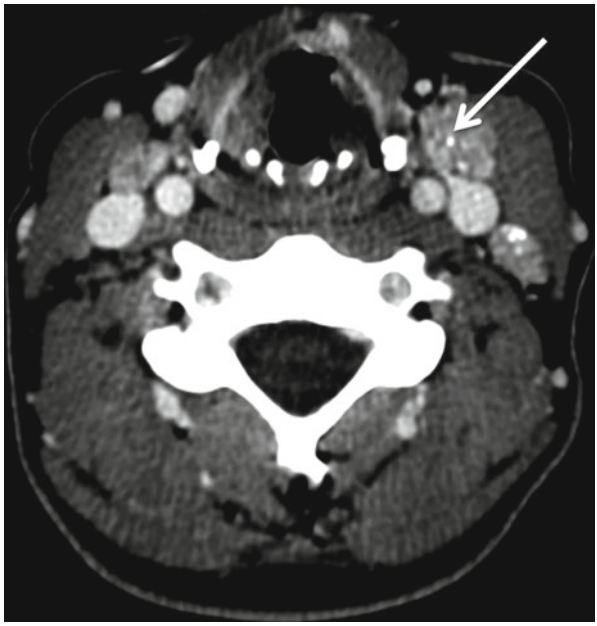

Fig. 2.18 Papillary carcinoma with nodes. Multiple small specks of calcification are seen in the abnormally enhancing left level IV nodes (*arrow*)

2.4.4 Tuberculous and Mycobacterial Lymphadenitis

Mycobacterial infections are divided into tuberculous and nontuberculous infections. Both most commonly involve infrahyoid nodes, with the internal jugular and posterior triangle nodes most frequently affected. Unlike patients with nonmycobacterial lymphadenitis, patients with tubercular adenitis have few generalized symptoms and may present with a painless neck mass. The imaging appearance depends on the stage on the infection: nodes are homogenously enhancing in the initial phase and then become centrally necrotic in the subacute phase with progression to fibrocalcific changes in the posttreatment or chronic state. On CT, the nodes may demonstrate variable enhancement with areas of nodal necrosis and

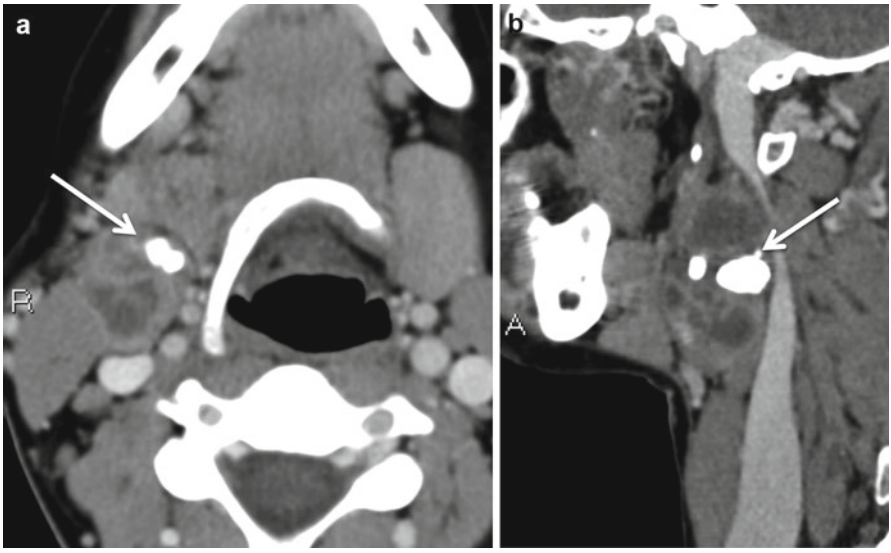

Fig. 2.19 (**a** and **b**) Known HIV positive patient with tuberculosis shows right level II necrotic node with thick calcification (*arrows*)

variable calcification (Fig. 2.19). Similarly, on MR, the nodes might appear complex depending on the stage of disease. Eggshell calcification, which is sometimes seen in tuberculous nodes, can be seen in silicosis and sarcoidosis.

Nontuberculous mycobacterial infections are the commonest granulomatous infection in children and are caused by *M. avium intracellulare*, *M. bovis*, and other nontuberculous mycobacterial species. The imaging findings are similar to tuberculous adenitis, commonly affecting children between 2 and 4 years of age.

2.4.5 Viral Infection

Viral infections including mononucleosis, HIV infection, and mumps generally present as bilateral diffuse lymphadenopathy without necrosis, similar in radiographic appearance to noninfectious causes such as lymphoma and sarcoidosis. Viral adenitis is also common in the pediatric age group, resulting in reactive lymphadenopathy. Tonsillar enlargement and large nodal lesions can be seen in patients with infectious mononucleosis (Fig. 2.20). HIV infection can have unique imaging signs, including enlarged adenoids and multiple bilateral benign intraparotid lymphoepithelial cysts (Fig. 2.21).

2.4.6 Other Inflammatory Conditions

Some of the other rare causes of lymphadenopathy include sarcoidosis, Langerhans cell histiocytosis, Castleman's disease (angiofollicular lymphoid hyperplasia), Kimura disease, Kikuchi disease, sinus histiocytosis with massive lymphadenopathy

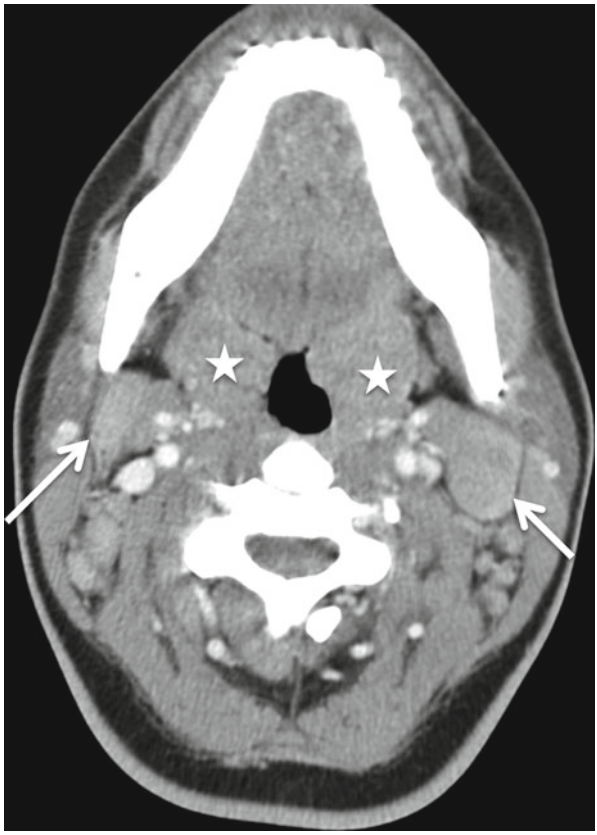

Fig. 2.20 Bilateral multiple enhancing nodes (*arrows*) with enlarged bilateral tonsillar tissue (*star*) are seen in this 19 years old with infectious mononucleosis

Fig. 2.21 A 25-year-old HIV patient with the classical imaging appearance of multiple bilateral benign intraparotid lymphoepithelial cysts (*arrows*)

(Rosai-Dorfman disease), and posttransplantation lymphoproliferative disease (PTLD) (see Box 2.1).

Common head and neck manifestations of sarcoidosis include cervical lymphadenopathy with parotid gland, facial nerve, ocular, and lacrimal involvement. The nodal disease in sarcoidosis is usually bilateral, non-tender, and non-necrotic with diffuse homogenous enhancement and well-defined margins. Eggshell calcification may be seen. The combination of bilateral enlarged parotids with bilateral nodal disease and pulmonary involvement suggests sarcoidosis.

Castleman's disease (angiofollicular hyperplasia) involves head and neck nodes in 10–15 % of cases and is usually of the hyaline-vascular subtype, which is characterized by vascular proliferation. Thus, involved nodes usually demonstrate intense contrast enhancement with a prominent adjacent vessel (Fig. 2.22).

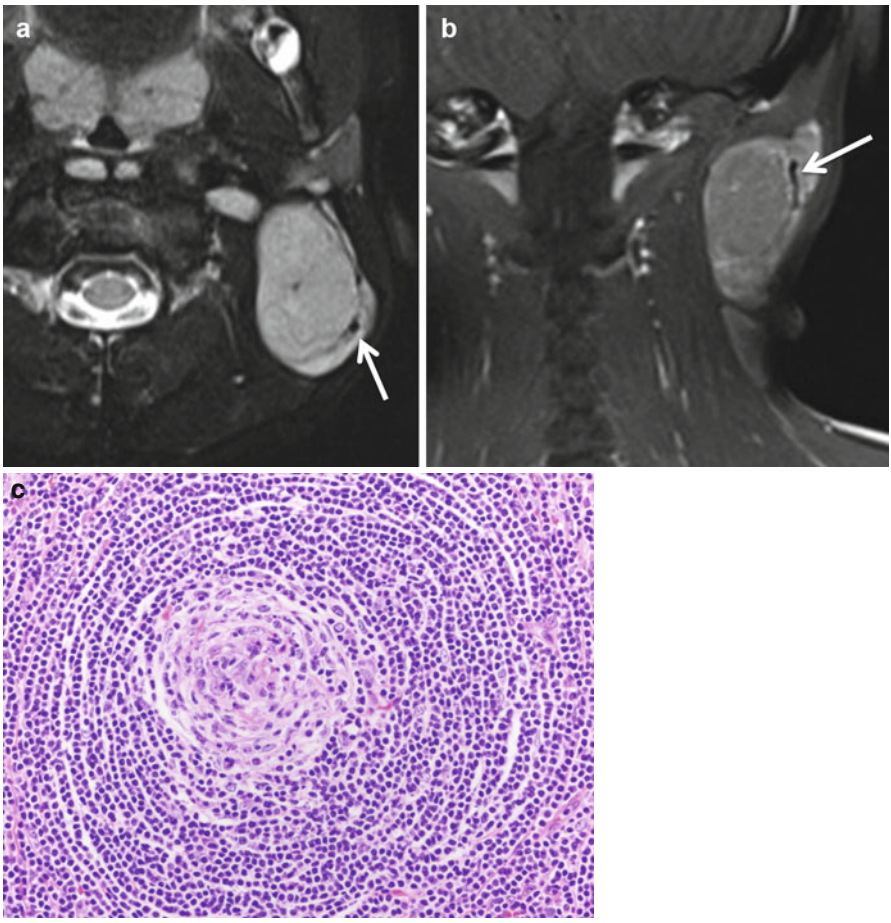

Fig. 2.22 Castleman's disease. Biopsy-proven hyaline-vascular variant of Castleman's disease in this young adult with persistent lymphadenopathy. Note the large dominant posterior neck node with the adjacent flow void. (*arrow* in **a** and **b**). The pathology slide (**c**) demonstrates the classical findings of lymphoid follicle with central hyalinized blood vessels and "onion skin" arrangement of lymhocytes in the hyaline vascular variant of Castleman's disease

Rosai-Dorfman disease (sinus histiocytosis with massive lymphadenopathy) is a rare benign histiocytic proliferation that occurs in young patients. It is characterized by massive painless cervical lymphadenopathy with homogenous enhancement. Associated orbital and salivary gland lesions are seen in 20–30 % of patients.

PTLD (posttransplant lymphoproliferative disease) can demonstrate cervical lymphadenopathy; it can present as a dominant large nodal mass with low central attenuation or as diffuse bilateral nodal disease (Fig. 2.23).

Kimura disease is an inflammatory disease seen in younger Asian men, consisting of cervical adenopathy, peripheral eosinophilia, and elevated serum IgE. Imaging findings of Kimura disease are nonspecific, but markedly enhancing nodes are common.

2.5 The Surgeon's Perspective

When evaluating a patient with cervical lymphadenopathy, imaging is a powerful tool, but clinical examination and patient context are paramount. While experienced examiners can identify cervical masses as enlarged lymph nodes, it is important to be aware that other neck structures, normal and abnormal, can masquerade as lymph nodes. For example, ptotic submandibular glands are common in elderly patients, and this diagnosis can be made clinically without costly imaging. Similarly, many thin

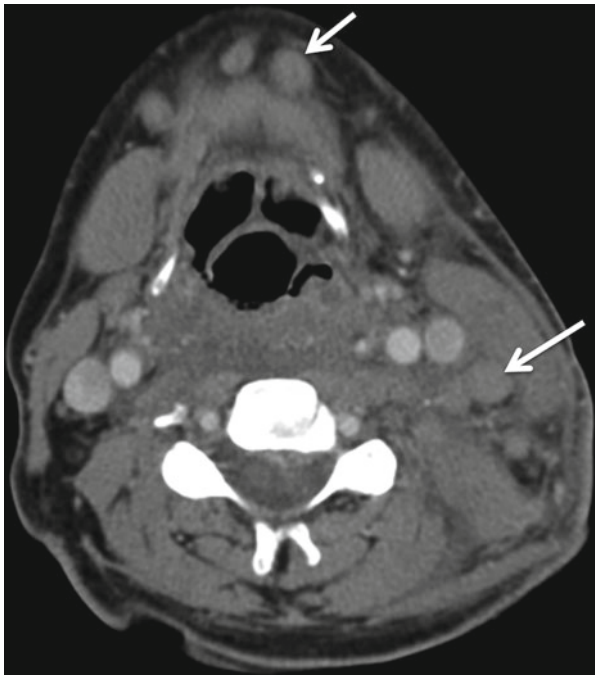

Fig. 2.23 Multiple hypo-enhancing nodes (*arrows*) are seen in this patient with PTLD (posttransplant lymphoproliferative disease). These lesions can present as both multiple small nodes and a large dominant nodal mass

patients have prominent carotid bulbs, and these should not be imaged (or biopsied!). In both scenarios, the patient context complements the clinical examination, and this information is valuable to not only the otolaryngologist but also the radiologist.

A middle-aged adult smoker with cervical lymphadenopathy has cancer until proven otherwise, and imaging and FNA biopsy are in order rather than one or more courses of antibiotics. Children and young adults (especially nonsmokers) with lymphadenopathy are more likely to have a benign infectious illness and, when the clinical context is clear, may be treated with appropriate medical care without imaging. When the imaging does not fit this picture and is more suggestive of malignancy, the radiologist must be aware that the most likely source is the upper aerodigestive tract, rather than metastasis from more distant sites, so that patients are sent on for evaluation by an otolaryngologist – head and neck surgeon in a timely fashion.

One must be aware of the increasing incidence of HPV-related oropharyngeal SCC, which often occurs in young adults with no smoking history. This disease is unique to HPV-negative SCC and often presents with a large cystic node and a very small primary tumor (Fig. 2.24). A common pitfall is to misdiagnose such a node as a branchial cleft cyst. First presentation of a branchial cleft cyst in an adult is extremely rare. Thus, detection of a cystic neck mass in an adult should prompt the radiologist to look for HNSCC, especially in the tonsils and tongue base. Even if the primary is not detectable on imaging, the radiologist should suggest thorough

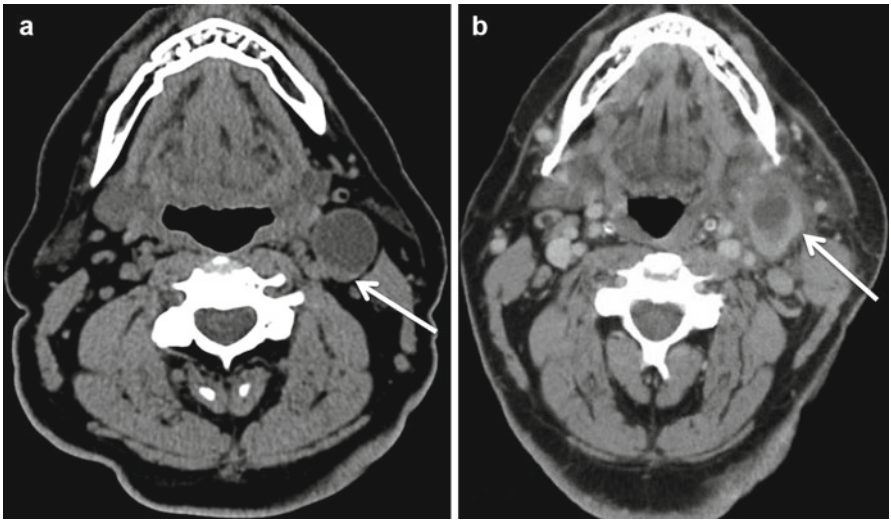

Fig. 2.24 A 45-year-old female who presented with a cystic left neck mass, (*arrow*) on contrast-enhanced CT scan (**a**), mimicking a branchial cleft cyst. Note the minimal soft tissue along the posterior margin. No identifiable primary was obvious on the scan. Speculative biopsies under endoscope revealed a left tonsillar primary. Radiologists should be aware of this pitfall in adult patients presenting with cystic level II lesion, which represents cystic nodal metastasis and is common in HPV-associated oral/oropharyngeal cancers. Infected branchial cleft cysts in adult patients can mimic the appearance of cystic necrotic nodes (*arrow* in **b**), although they are quite rare

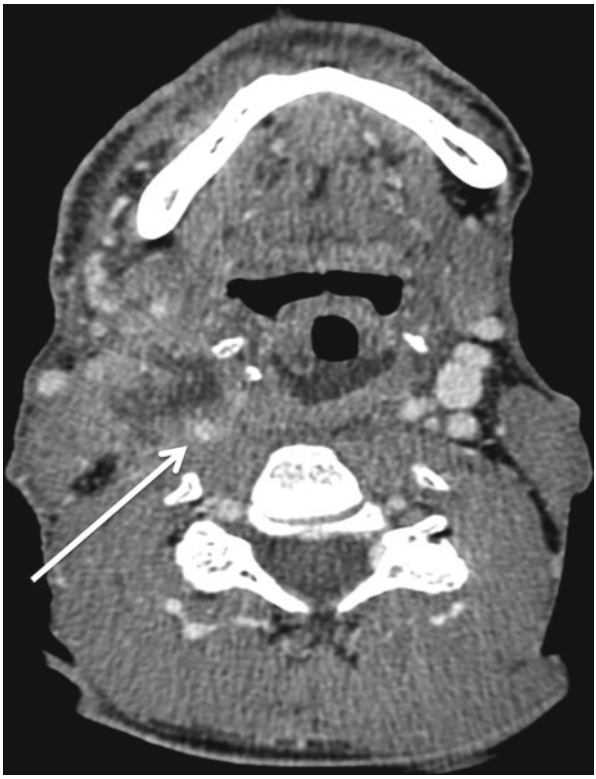

Fig. 2.25 Right carotid sheath invasion is seen in this patient with recurrent right-sided neck disease. Note the lack of tissue planes and loss of fat adjacent to the carotid sheath, with occluded jugular vein (not visible) and a visibly narrowed right carotid artery (*arrow*)

endoscopic evaluation of the oropharynx and FNA biopsy of the node. This approach will often be futile without ultrasound guidance, which allows for specific sampling of the solid cancerous rim of the node. Incorrect diagnosis of these nodes as branchial cleft cysts obviously leads to unnecessary delay in treatment of the patient's HNSCC.

With few exceptions (e.g., T1 glottic SCC), CT or MR imaging are a necessary component of staging for head and neck cancers. While it is important to carefully evaluate all neck levels for nodal abnormalities, it is useful to be well versed in the predicted nodal drainage patterns so that, given a specific primary, the status of the most likely nodal targets can be clearly delineated (Box 2.3). When nodes at the expected regional metastasis locations exhibit borderline or equivocal characteristics, this should be reported as it may impact clinical management. Several features of nodal metastases should be communicated because they impact prognosis and management. The number of positive nodes should be clearly delineated, as the presence of multiple nodes often indicates the need for dual modality therapy for that side of the neck. The presence of ECS is a high-risk feature that warrants additional therapy. The presence of carotid encasement or invasion, or extension to or involvement of the skull base, or prevertebral space may render the patient inoperable and dramatically change treatment planning (Fig. 2.25).

Box 2.3. Most Frequently Affected Nodal Levels by Head and Neck Cancers

Location of primary cancers	Most frequently involved nodal stations
Floor of mouth and oral tongue	Ipsilateral levels I and II
Base of tongue and tonsils	Ipsilateral levels II and III and contralateral level II
Soft palate	Ipsilateral and contralateral level II, ipsilateral level III
Nasopharynx	Ipsilateral and contralateral levels I and V
Supraglottic larynx	Ipsilateral levels II and III and contralateral level II
Glottis	Ipsilateral levels II and III

HNSCC can present with metastatic lymph node(s) only and no identifiable primary on physical exam (unknown primary, T0). Again, a thorough knowledge of the lymphatic drainage pathways is extremely helpful, in this setting to identify the primary (Box 2.3). Primaries that are not detectable on physical exam are often identifiable on high-resolution CT or MR imaging; PET/CT can be additionally helpful in identifying very small primaries, often within lymphoid tissue. Findings on these studies can guide biopsies and result in a higher rate of primary identification, which allows for more focused therapy, rather that the broad radiation to Waldeyer's ring that is required for primaries that cannot be formally diagnosed. HPV and EBV testing of the nodal biopsy can also be helpful in directing the search for the primary. It is important to remember that, in rare cases, the primary is outside the head and neck region, requiring a whole-body work-up.

Management of the cervical nodes is warranted in patients staged N1 or greater or in patients stage N0 who carry a greater than 20 % risk of occult nodal metastasis (Box 2.4). Neck nodes can be treated with radiation or surgically by neck dissection (ND), which involves removal of the fibrofatty tissue of the neck in which the nodes reside. NDs can be therapeutic (for N+ disease) or prophylactic (for N0 disease) and are classified as radical, modified radical (comprehensive), selective, or extended. Box 2.5 summarizes the neck dissection terminology and definitions. Imaging in these cases would reveal deformity, loss of normal contour, and tissue planes in the neck along with absence of the removed nonlymphatic structures. Given the extent of surgery in extended ND, this is reserved for special cases with bulky nodal disease and/or extranodal spread and often requires some form of reconstruction.

Box 2.4. American Joint Committee on Cancer Nodal Staging and Features in Head and Neck Cancers

Stage N0	No nodes
Stage N1	Single, ipsilateral node $\leq$3 cm
Stage N2a	Single, ipsilateral node >3 cm and $\leq$6 cm
Stage N2b	Multiple, ipsilateral nodes $\leq$6 cm
Stage N2c	Bilateral, or contralateral nodes $\leq$6 cm
Stage N3	Nodal metastases >6 cm

Adjusted from American Joint Committee on Cancer Staging (2010) American Joint Committee on Cancer Staging manual. 7th edn. Springer

Box 2.5. Summary of Neck Dissection Terminology and Definitions

Type of neck dissection	Lymph node Levels removed	Nonlymphatic structures removed
Radical neck dissection (RND)	I, II, III, IV, V	Sternocleidomastoid muscle, internal jugular vein, spinal accessory nerve
Modified radical neck dissection (MRND) (includes functional neck dissection)	I, II, III, IV, V	Sparing at least 1 of the following: Sternocleidomastoid muscle, internal jugular vein, spinal accessory nerve
Extended neck dissection (END)	I, II, III, IV, V, and additional nodal stations	Structures removed in RND and additional structures such as carotid artery, overlying skin, strap and paraspinal muscles, platysma, and hypoglossal and vagus nerves

Many HNSCCs are treated with definitive radio- or chemoradiotherapy (C/RT). There is a substantial body of literature that supports observation if nodal metastatic disease is completely resolved on post-C/RT imaging. If post-C/RT imaging demonstrates persistent soft tissue concerning for residual malignancy, options include (1) empiric ND, which often yields no viable tumor; (2) directed needle biopsy, which has a high false-negative rate in the setting of microscopic residual disease; or (3) functional imaging with PET/CT, which has a very low false-negative rate but a high false-positive rate before 12 weeks posttreatment and thus can result in delayed ND in the setting of persistent disease. The approach in these cases varies by institution and surgeon (Box 2.6).

Box 2.6. Pearls and Pitfalls

- Know the landmarks for nodal stations and where different cancer subsites drain
- Comment on extracapsular extension, unilaterality/bilateral and contralateral, presence of nodes while describing nodal involvement in head and neck cancers, etc.
- Always remember to look for commonly missed nodal disease, e.g., retropharyngeal nodes
- Parotid lymph nodes represent the primary site for drainage of skin cancers from the scalp and skin cancers of the adjacent region. Skin cancers can also metastasize to level V and other superficial nodes, such as postauricular, facial, and occipital nodes
- Know about imaging appearance of HPV-related oral/oropharyngeal cancer-related cystic nodes (potential mimic for type 2 branchial cysts in young adults).

Further Reading

Som PM, Curtin HD, Mancuso AA (2000) Imaging-based nodal classification for evaluation of neck metastatic adenopathy. AJR Am J Roentgenol 174:837–844